# COMPANION EVENT AND PRECURSOR OF THE X17 FLARE ON 28 OCTOBER 2003

C.H. MANDRINI

*Instituto de Astronomía y Física del Espacio (IAFE), CONICET-UBA, CC. 67, Suc. 28, 1428, Buenos Aires, Argentina*
*(e-mail: mandrini@iafe.uba.ar)*

P. DEMOULIN and B. SCHMIEDER

*Observatoire de Paris, LESIA, FRE 2461 (CNRS), F-92195 Meudon Principal Cedex, France*
*(e-mails: pascal.demoulin@obspm.fr, brigitte.schmieder@obspm.fr)*

E.E. DELUCA

*Smithsonian Astrophysical Observatory (SAO), MS 3, 60 Garden Street, Cambridge, MA 02138, U.S.A.*
*(e-mail: edeluca@cfa.harvard.edu)*

E. PARIAT

*Observatoire de Paris, LESIA, FRE 2461 (CNRS), F-92195 Meudon Principal Cedex, France*
*(e-mail: etienne.pariat@obspm.fr)*

and

W. UDDIN

*Aryabhatta Research Institute of Observational Sciences (ARIES), Manora Peak, NainiTal 263 129, India*
*(e-mail: wahab@upso.ernet.in)*

**Abstract.** A major two-ribbon X17 flare occurred on 28 October 2003, starting at 11:01 UT in active region NOAA 10486. This flare was accompanied by the eruption of a filament and by one of the fastest halo coronal mass ejections registered during the October–November 2003 strong activity period. We focus on the analysis of magnetic field (SOHO/MDI), chromospheric (NainiTal observatory and TRACE), and coronal (TRACE) data obtained before and during the 28 October event. By combining our data analysis with a model of the coronal magnetic field, we concentrate on the study of two events starting before the main flare. One of these events, evident in TRACE images around one hour prior to the main flare, involves a localized magnetic reconnection process associated with the presence of a coronal magnetic null point. This event extends as long as the major flare and we conclude that it is independent from it. A second event, visible in Hα and TRACE images, simultaneous with the previous one, involves a large-scale quadrupolar reconnection process that contributes to decrease the magnetic field tension in the overlaying field configuration; this allows the filament to erupt in a way similar to that proposed by the breakout model, but with magnetic reconnection occurring at Quasi-Separatrix Layers (QSLs) rather than at a magnetic null point.

## 1. Introduction

After 19 October 2003, and for about two weeks, the Sun displayed an extraordinary level of activity. Twelve X-class (X-ray GOES classification) flares and many

smaller ones (lower class) were observed. Other phenomena were associated with these flares, including coronal mass ejections (CMEs) and strong fluxes of accelerated particles (electrons, protons, and neutrons). The extremely high level of activity resulted from the formation of three $\beta-\gamma-\delta$ sunspot groups (NOAA 10484, 10486, 10488). Eight of the X-flares started in active region (AR) 10486. Various aspects of this activity period have been investigated in special issues of the *Journal of Geophysical Research*, *Geophysical Research Letters* and *Space Weather* published in 2004 and 2005 (see *http://www.agu.org/journals/ss/VIOLCONN1/*). The complexity of the X17 flare on 28 October was analyzed in H$\alpha$, radio, and white-light images by Pick *et al.* (2005), and the coronal magnetic structure was linked to the associated interplanetary magnetic cloud by Yurchyshyn, Hu, and Abramenko (2005).

There are a number of conditions, inferred from observations, that are necessary for the production of flares and CMEs: complex magnetic topology of the AR, such as the so-called $\delta$ configurations in which umbrae of opposite polarities share a common penumbra; a high level of stored energy by shear, twist, or emerging flux; and a strong magnetic field (see, *e.g.*, Schmieder and van Driel-Gesztelyi, 2005, for a review).

Most models for the initiation of flares and/or CMEs share the assumption that the stored magnetic energy lies in a low-lying magnetic flux system (sheared or twisted). The topology of this system can be basically of two types: either a sheared magnetic arcade extending along the magnetic inversion line or a core flux rope that lies above the inversion line, a combination of both topologies is also invoked. In general, models differ in the way the flare and/or CME is initiated and, also, in the precise role played by the overlaying field (see Klimchuk, 2001, for a review on CME models).

Forbes and Isenberg (1991), Lin *et al.* (1998), and references therein, developed flux-rope models of CMEs. In these models, the eruption is preceded by converging photospheric motions towards the magnetic-inversion line, as is sometimes observed (*e.g.*, van Driel-Gesztelyi, Schmieder, and Poedts, 2002, and references therein). When the footpoints of the field lines reach the inversion line, reconnection under the flux rope occurs. When enough arcade lines have been converted into flux rope lines, a loss of equilibrium leads to the rise of the flux rope. In the breakout model, magnetic reconnection above an expanding arcade is the key ingredient (Antiochos, DeVore, and Klimchuk, 1999). This process decreases the stabilizing magnetic tension above the extremely sheared central arcade and an eruption finally starts. Aulanier *et al.* (2000) combined multiwavelength observations with magnetic field modelling to provide the first observational evidence that the breakout model is viable for CMEs, though a more convincing example has been analyzed by Gary and Moore (2004) and Harra *et al.* (2005). In some simulations, the emergence of a flux rope from below the photosphere induces a kink instability (Fan and Gibson, 2004; Gibson *et al.*, 2004). This instability also appears in some coronal models of twisted configurations and can lead to a CME (Kliem, Titov, and

Török, 2004). The observed characteristics of some CMEs, such as the formation of a helically-shaped structure and the rise of the velocity profile of the ejected structure, have been reproduced by simulations (Török and Kliem, 2005; Williams *et al.*, 2005).

Magnetic-field studies concerning AR 10486, its evolution, and its relationship to the X17 flare on 28 October, have already been done. Wang *et al.* (2004) showed evidence that penumbral segments decayed rapidly after the X17 flare; they interpreted this as a change from a highly-inclined to a more vertical magnetic configuration. Régnier and Fleck (2004), using a non-linear force-free field extrapolation method, based on Imaging Vector Magnetograph observations, computed the topology of the field and its energy content. Schmieder *et al.* (2006) proposed that large-scale quadrupolar reconnection in the AR, prior to the X-flare, could be at the origin of its occurrence. In this paper, we extend this preliminary study.

We concentrate on the analysis and interpretation of two events that started before the 28 October 2003 X17 flare. It is not our aim to deal with the flare itself, though the movies (ESM[1]) that accompany this paper will include its evolution. We identify one of these events with the precursor of the two-ribbon flare, while the second one accompanies the major flare during its entire duration and seems to be completely independent of it. We combine data analysis with magnetic-field modelling and a study of the AR topology, which helps us to disentangle and associate the appearance of different brightenings with different events. In Section 2, we describe the observations that will be the basis of the physical interpretation proposed in Section 3. Finally, in Section 4, we discuss our results related to the pre-eruption configuration.

## 2. Observational Characteristics of the Events Linked to the X17 Flare

### 2.1. INSTRUMENTS AND DATA

During October and November 2003, solar instruments, ground-based as well as space-borne, were devoted to the observation of ARs 10484, 10486, and 10488.

We use here magnetic field observations from the Michelson Doppler Imager (MDI; Scherrer *et al.*, 1995) aboard the Solar and Heliospheric Observatory (SOHO). These are full-disk level-1.5 magnetic maps, which are the average of five magnetograms with a cadence of 30 seconds. They are constructed once every 96 minutes. The error in the flux densities per pixel in the averaged magnetograms is about $\pm 9$ G, and each pixel has a mean area of $1.96\,\text{Mm}^2$.

For the chromospheric data, we use H$\alpha$ observations from the ARIES Observatory at NainiTal, India, taken on 28 October 2003. These are images obtained with a 15-cm telescope and have a temporal cadence of 25 ms.

[1]Electronic Supplementary Material (ESM) is available for this article at http://dx.doi.org/10.1007/s11207-006-0205-3.

Transition region and coronal observations, and also chromospheric data, come from the Transition Region and Coronal Explorer (TRACE; Handy *et al.*, 1999). TRACE observed with high temporal cadence (60 seconds) in the 1600 and 195 Å passbands with an FOV of $768'' \times 768''$ before 11:00 UT and after 12:00 UT on 28 October. A lower temporal cadence was used for the 284 Å passband between 09:30 and 11:00 UT, while a higher one (4 seconds) was chosen in 195 Å (flare-watch mode) between 11:00 and 12:00 UT. Finally, from 14:00 to 17:00 UT TRACE observed in three passbands (5000, 1600, and 1700 Å). The pixel size in all images is $0.5''$, giving a spatial resolution of $1.0''$.

The plasma observed by TRACE in the 1600 Å bandpass has temperatures in the range of $(4.0 - 10) \times 10^3$ K (Table I of Handy *et al.*, 1999), these temperatures correspond to the upper photosphere and chromosphere. As the spots are clearly visible in these images, they have been used to coalign TRACE images with MDI magnetic maps (see Figure 3).

## 2.2. THE MAGNETIC FIELD EVOLUTION

AR 10486 arrived at the east solar limb on 23 October 2003, with an already complex magnetic configuration. Figure 1 shows the evolution of the region between 25 and
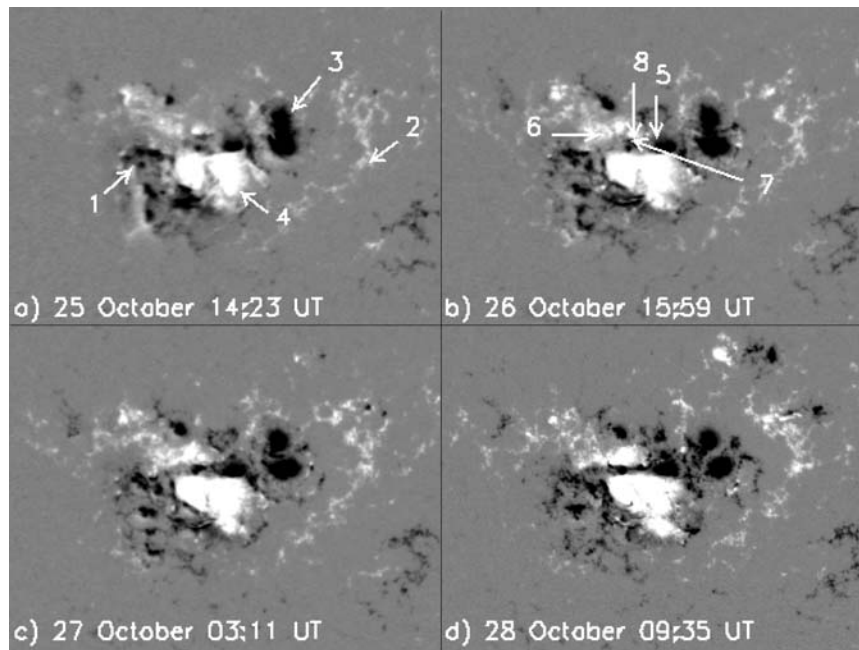


*Figure 1.* Magnetic field evolution from 25 to 28 October 2003. MDI magnetic maps showing the evolution of the polarities that could be involved in the two events discussed in this paper. The polarities (marked by *arrows*) are numbered as described in Section 2.2. The area covered by the images is 305 × 229 pixels ($603'' \times 453''$). The magnetic field values are saturated above (below) 500 G ($-500$ G). In this and all figures depicting the observations, solar North is to the *top* and West is to the *right*.

28 October. An extended and high-intensity field bipole (polarities 3 and 4 in Figure 1a) emerged when the AR was still on the far side of the Sun; the emergence occurred within a mainly negative field environment (to which polarity 1 belonged). The leading polarity 3 lay very close to the trailing positive polarity of an already decayed AR (polarity 2).

The new emerging bipole (polarities 3 and 4) consisted initially of one preceding sunspot of negative polarity and two following spots of positive polarity. This emerging bipole followed the Hale–Nicholson polarity law (Hale and Nicholson, 1925). The preceding spot grew and separated in two on 26 October, while the following part continued its disk transit having two spots with increasing strength. To the north of the positive polarity, several bipoles emerged. Polarities 5 and 6 (Figure 1b) were already visible when the AR appeared on the east limb and they continued growing in intensity as it approached its central meridian passage. On 26 October, a very small bipole (polarities 7 and 8 in Figure 1b), which started to emerge on 25 October (Figure 1a), was clearly above the main inversion line (Li *et al.*, 2006). All of this field emergence created a positive island (formed by the merging of 6 and 8) separated from the main positive spots by a negative bridge (formed by the merging of 5 and 7).

By 28 October, the AR was formed by four extended polarities defining a large quadrupolar magnetic configuration (Figure 1): two negatives (1 and 3+5+7) and two positives (4 and 6+8). The onset of the large X17 flare, at 11:01 UT, occurred along the inversion line between the negative bridge (polarities 5+7) and the positive spots (polarity 4), at that time AR 10486 was located at S17 W09.

THEMIS in Tenerife also observed AR 10486 on 28 October with its Multi-Channel Subtractive Double Pass instrument (Mein, 2002); the configuration just described is also visible with higher spatial resolution in its longitudinal-magnetic-field maps (Schmieder *et al.*, 2006). Several other minor emergence episodes occurred during the passage of this complex AR across the disk until its disappearance on the west limb on 4 November 2003. A movie of AR 10486 magnetic field evolution from 23 October to 4 November is available as ESM (*MDI-evol.avi*).

## 2.3. THE LARGE-SCALE EVENT

A large, sigmoidal filament in the central part of the region separated the leading negative spots and the main following positive spots (see top image in Figure 2). This filament was already visible in Hα images obtained with the Meudon Observatory Spectroheliograph on 25 October (see *http://mesola.obspm.fr/*). In an Hα movie from NainiTal observatory, which observed from the early morning (01:28 UT) on 28 October to the flare decay phase, we observe different features before the two-ribbon flare:
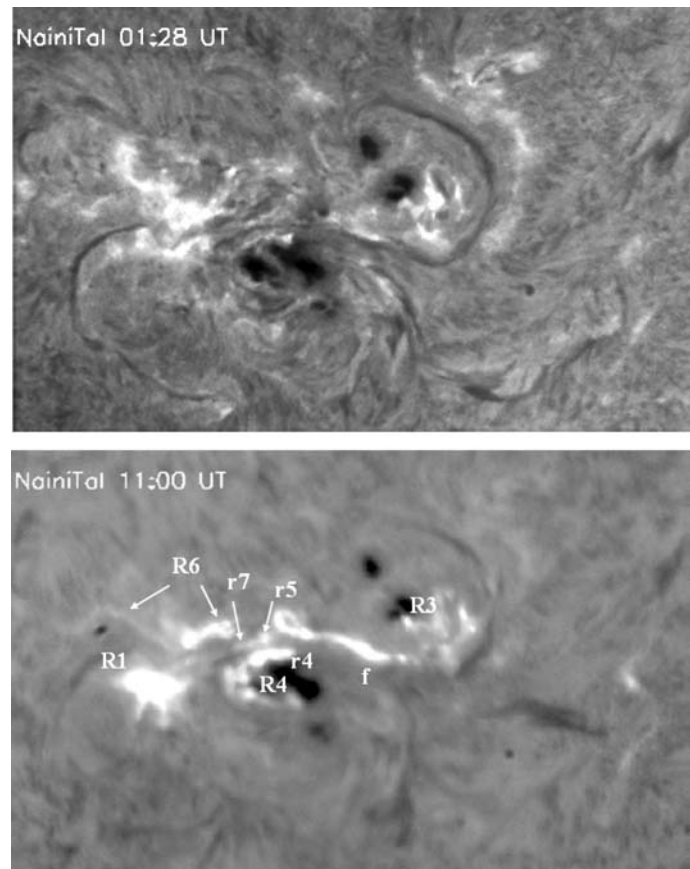
*Figure 2.* Images showing a large-scale view of the AR in Hα. An elongated sigmoidal filament is seen on the *top*, the eruption of its central portion accompanies the two-ribbon X17 flare. The image at the *bottom* shows the Hα ribbons with their associated label starting with "R" and "r" for those associated with a large-scale event (Section 2.3) and a small-scale event (Section 2.4), respectively. The number in the ribbon label indicates the magnetic polarity defined in Figure 1. "r4" has merged with "R4" in this image and other brightenings are present to the west of "R3" (compare to Figure 3). The letter "f" refers to the heated filament plasma.

– A surge ejection towards the south west in front of the following spots at 08:09 UT. This surge was also observed in Hα at the Meudon Observatory.
– Four bright, well-separated ribbons (called R1, R3, R4, and R6 Figure 2, bottom) together with an elongated brightening that lay along the main inversion line. This later brightening is interpreted as the emission of the heated filament plasma ("f" Figure 2, bottom). The four ribbons are also visible in Meudon Hα images at ∼10:59 UT. At the same location, four bright plage patches were observed previously in the Hα image at 01:28 UT (Figure 2 top).

– The ejection of the central part of the sigmoidal filament that is not radial but inclined towards the south west.

Four ribbons are also evident in TRACE images, 1600 Å bandpass, 1 hour before the initiation of the two-ribbon flare (R1, R3, R4 and R6 in Figure 3, top). We
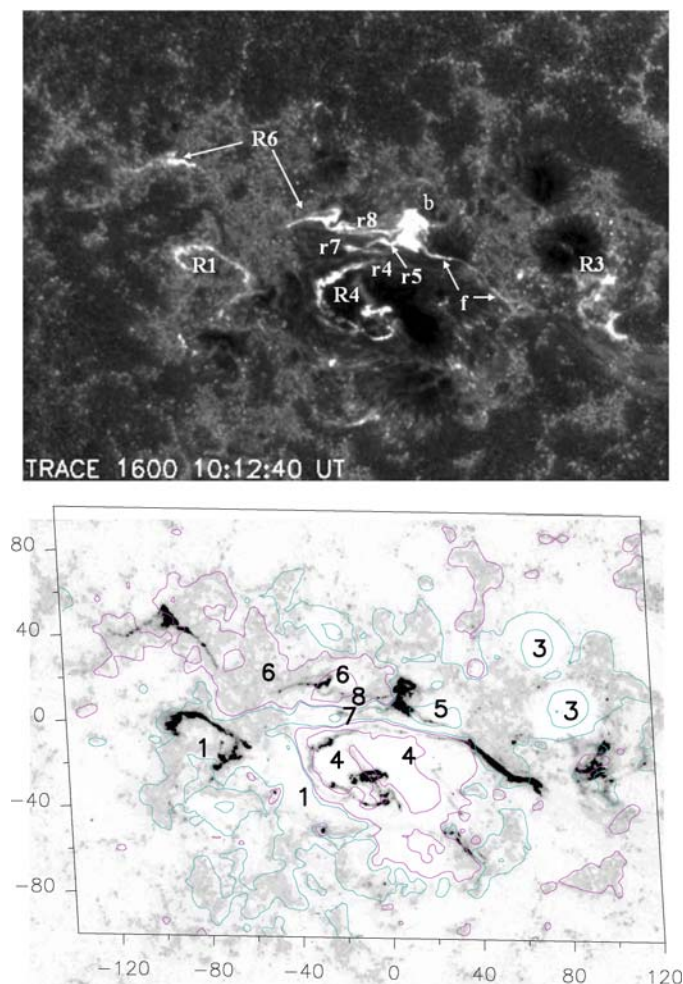


*Figure 3.* TRACE 1600 Å image. The *top* figure shows the four ribbons for both the large-scale and small-scale events: R1, R3, R4, R6, and r4, r5, r7, r8, respectively. They correspond to the Hα ones observed in Figure 2. The top (bottom) figure is in direct (reverse) intensity scale. Other brightenings are also present at this time: "b" marks a localized brightening that we interpret as linked to energy release in a small mixed polarity region, "f" points to the filament brightening (better seen in the reverse intensity image in the bottom figure). The image is $767 \times 548$ pixels ($384'' \times 274''$) in size. The bottom figure corresponds to the overlay with the MDI magnetogram at 11:11 UT. The axes *x* and *y* are labeled in Mm. The isocontours of the field are $\pm 100$ and 1000 G, shown with continuous *pink* (*blue*) lines for the positive (negative) values. Polarities are numbered as in Figure 1.

identify these four ribbons with the ones observed in Hα. The central–northern ribbon (R6) is very elongated and all along polarity 6, which had already merged with 8 at the time of the MDI map (28 October, 11:11 UT). The south eastern ribbon (R1) has an inverse U shape. To the west, a very concentrated ribbon (R3) lies to the south of the big southern negative spot. Finally, a fourth ribbon (R4) is seen following the inversion line surrounding the positive spot. The temporal evolution of TRACE emission in 1600 Å can be followed in the movie (*ESM, 1600-evol.avi*) that accompanies this paper.

## 2.4. THE SMALL-SCALE EVENT

Around 1 hour before the initiation of the X17 flare, bright coronal emission was observed by TRACE in 195 Å close to the location where polarities 7 and 8 emerged. These localized brightenings had the shape of curved loops extending above the inversion lines separating the negative tongue from the positive polarities northward and southward (Figure 4, top). These loops were associated with four ribbons (r4, r5, r7, r8), as shown in Figure 3, just as expected in an event where reconnection has occurred (each pair of ribbons is associated with a set of reconnected field lines).
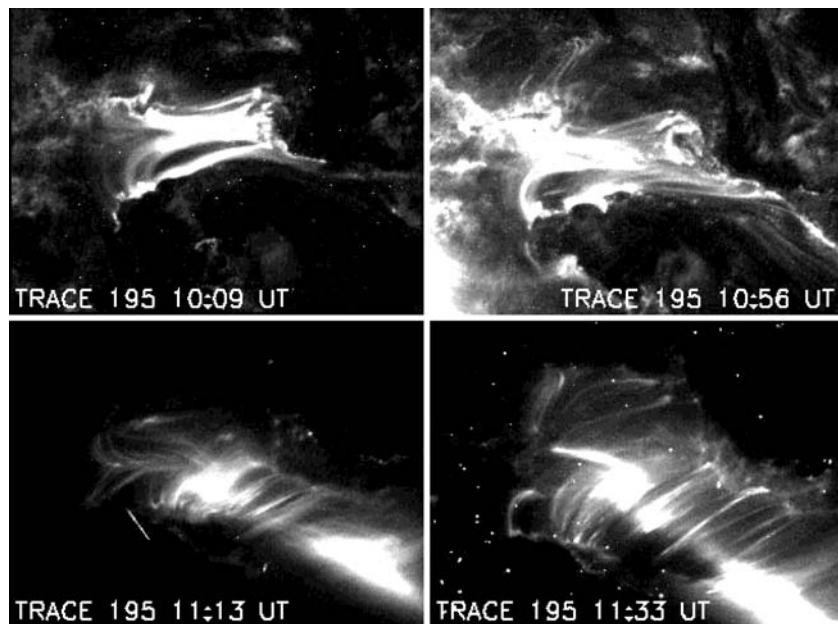


*Figure 4.* TRACE 195 Å images. This series of images shows the evolution of the localized event, related to the emergence of polarities 7 and 8 (Section 3.3), at different times before and during the two-ribbon flare (compare TRACE loops to the field lines in Figure 8). The field of view is 316 × 235 pixels (158″ × 118″).

The shape of these brightenings can be followed at different times during the X17 flare (*e.g.*, Figure 4, bottom left) and even during its decay phase (Figure 4, bottom right). Then, they are difficult to see and appear blurred by the bright post-flare arcade formed during the two-ribbon flare. The temporal evolution of the TRACE emission in 195 Å can be seen in the *ESM* movie, *195-evol.avi*. Brightenings in Hα at similar locations also occurred, at least one day earlier, during the M6.7 flare at 12:13 UT on October 27 (Luoni, Mandrini, and Démoulin, 2006). This indicates that these small-scale reconnection events are characteristics of the evolution of the magnetic configuration well before the X17 flare on October 28.

The early appearance and location of these loops, their peculiar shape, and their persistence during the X17 flare are difficult to understand if we consider them as a consequence of a reconnection process directly related to the two-ribbon flare. In Section 3.3, we present an interpretation based on a careful study of the magnetic field topology in their neighborhood.

## 2.5. OTHER BRIGHTENINGS

Other small brightenings, which complete the description of the observations, are also seen (Figures 2 and 3). Some of them follow the filament location and are interpreted as small reconnection events in the mixed polarity field present around the main inversion line. The filament itself appears in emission from time to time before the X17 flare (for example see "f" in Figure 3).

Brightenings are also visible to the south of R3. They correspond to two small ribbons in Figure 3. Furthermore, a concentrated brightening (called "b" in Figure 3) is present between polarities 5 and 6. In both cases, the emission is present above a mixed polarity magnetic field (*ESM, MDI-evol.avi*). These emissions are most likely due to the localized energy release associated with the complex local magnetic topology.

## 3. Physical Interpretation of the Events Linked to the X17 Flare

### 3.1. THE CORONAL-FIELD MODEL

To understand the origin of the emission described in the previous sections and its relation with the three-dimensional AR magnetic structure, we have extrapolated the observed, photospheric, longitudinal field to the corona. A force-free field configuration ($\mathbf{J} \times \mathbf{B} = 0$, $\nabla \times \mathbf{B} = \alpha B$), which corresponds to $\mathbf{J}$ parallel to $\mathbf{B}$ (*e.g.*, Metcalf *et al.*, 1995), is commonly assumed because of the low plasma $\beta$ (ratio of the plasma to the magnetic pressure). In this paper, we compute the coronal magnetic field under the linear (or constant $\alpha$) force-free field assumption following the method described by Démoulin *et al.* (1997), which is based on a fast Fourier

transform as proposed by Alissandrakis (1981). Our model takes into account the transformation of coordinates from the AR location to disk center.

We have taken, as a boundary condition for our coronal model, the MDI longitudinal magnetogram closest in time to the events studied. However, the magnetogram at 11:11 UT presents pixels with unphysical field values (within polarities 3 and 4). These unphysical values are due to the flare-induced disturbances (*e.g.*, Qiu and Gary, 2003); notice that the flare started at ~11:01 UT and had its maximum in X-rays at ~11:10 UT. We have modified the values in the "wrong" pixels by interpolating between the closest undisturbed pixels. As a check of our corrections, we have compared our interpolated values to the magnetic field values in the two MDI maps closest to the one at 11:11 UT, the one at 9:35 UT and the one at 12:47 UT. The resulting map is shown in Figure 5.

Our magnetic-field model depends on the free parameter $\alpha$. As shown in Huairou magnetograms, the AR field is highly non-potential (Zhang *et al.*, 2003). That is why, in this particular case, we have taken the largest possible value of $\alpha$ allowed by our model for the size of our integration box; this box includes all of the AR polarities and is large enough to avoid aliasing effects (see the discussion by Démoulin *et al.*, 1997, and the appendix in Green *et al.*, 2002). This value is $\alpha = -1.6 \times 10^{-2}\,\mathrm{Mm}^{-1}$. The computed model gives quite a good fit to the loops observed by TRACE in 195 Å, which are described in Section 3.3, and also to the loops connecting polarities 1 and 4 seen in the TRACE movie (*ESM, 195-evol.avi*) at ~10:47 UT.

The magnetic field model gives us information about the magnetic complexity of the AR in the corona and allows us to find clues about the location of the possible reconnection sites, as explained next.

## 3.2. THE LARGE-SCALE QUADRUPOLAR EVENT

Figure 5 (top) shows the large-scale coronal connectivity in AR 10486. The field lines have been computed starting integration at the photospheric level at, or in, the close vicinity of the four ribbons described in Section 2.3. It can be seen that our computed field lines connect these ribbons in pairs. The continuous, thin, blue field lines to the east connect R1 to R6, while the ones to the south west connect R3 to R4. In an analogous way, ribbons lying on polarities 6 and 3 can be connected by the thick, red field lines to the north, while those lying on polarities 1 and 4 are linked by the thick, red field lines to the south. This defines four connectivity regions.

The observed coronal connectivities, combined with the evolution observed in the movie *ESM, 1600-evol.avi* and the Hα observations, strongly suggests that the four ribbons are the result of magnetic field reconnection occurring at coronal heights.

As reconnection proceeds, it transforms the connectivity of the field lines that have footpoints at the border of the connectivity regions. The two regions
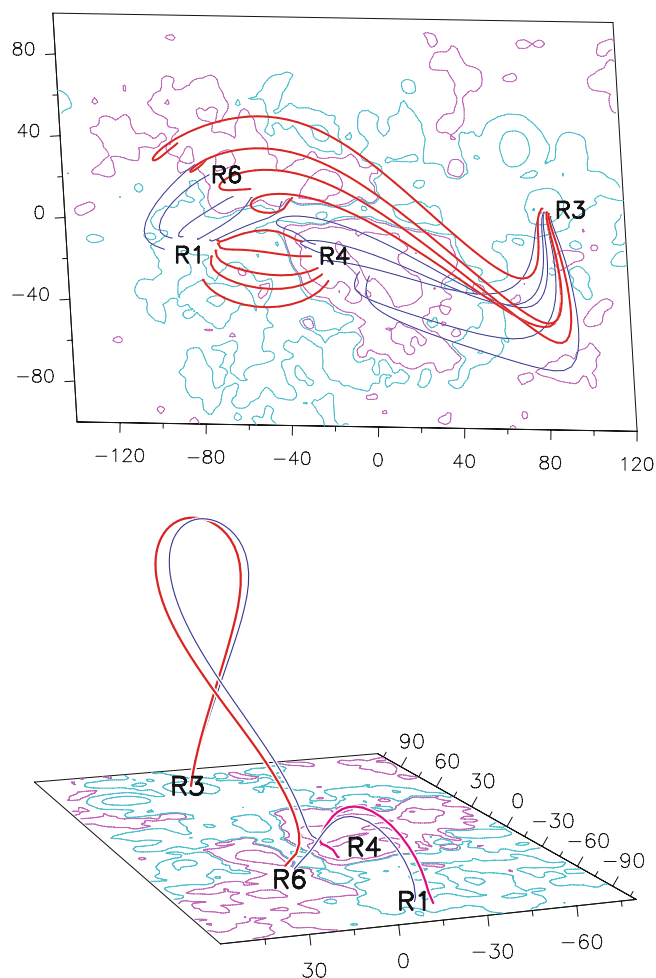
*Figure 5.* Coronal magnetic field model of AR 10486. The *top* panel shows the large-scale coronal connectivity from the observer's point of view. The computed field lines have footpoints located at or in the close vicinity of the four ribbons (R1, R3, R4, and R6) described in Section 3.2 and presented in Figure 3. Drastic changes in the field-line connectivity are present (defining QSLs). The *bottom* panel shows four field lines selected from the ones in the top figure from a different point of view. They have been computed starting the integration at coronal heights at the location where magnetic field reconnection could have started. In both figures, the field lines drawn with *thin, continuous, blue lines* correspond to the original magnetic connectivity, and the ones in *continuous thick red lines* to the connectivity after reconnection. The axes are labeled in Mm and the isocontours of the field correspond to ±100, 1000 G in continuous *pink* (*blue*) style for the positive (negative) values.

corresponding to the pre-reconnected (reconnected) field lines decrease (increase) in extension. This evolution is directly related to the motion of flare ribbons, which is difficult to detect in the event studied here. In this particular case, reconnection would have proceeded in a way that field lines anchored in 1 and 6 would reconnect

to those anchored in 3 and 4. This sequence in the reconnection process explains the appearance of loops connecting 1 to 4, which are clearly visible in 195 Å images at ∼10:47 UT (*ESM, 195-evol.avi*). Furthermore, the shape of our computed field lines connecting 1 to 4 are quite in agreement with the 195 Å loops. Finally, the Hα large ribbon on polarity 1 could be a combination of emission coming from the chromospheric footpoints of loops and that of evaporated material flowing along the newly formed loops.

We suggest that this reconnection process was steadily at work with low energy release since the early morning on 28 October, as suggested by the presence of the intense plage brightenings in the Hα image at 01:28 UT (Figure 2). This reconnection progressively removed the arcade field above the filament. When enough stabilizing field was removed, the filament magnetic configuration erupted.

The above scenario was proposed for the initiation of CMEs by Antiochos, DeVore, and Klimchuk (1999). However, this model invokes the presence of a magnetic null point above a strongly-sheared arcade (where the filament is supposed to lie). Despite an intensive search, we have not found such a null point in relation to the field lines that link the four observed ribbons. This could be attributed to the limitations of our magnetic extrapolation; however, we have found locations where continuous, but drastic, changes of connectivities are present. This is illustrated in Figure 5 by both an ensemble of field lines seen from the observer's view point and by an example of four field lines coming close to each other in the corona. The thin coronal volumes, where field lines locally display strong connectivity gradients, define Quasi-Separatrix Layers (QSLs, Démoulin *et al.*, 1996). QSLs generalize the definition of separatrices to cases where no coronal magnetic null is present and, so, they are the sites where magnetic field reconnection will naturally occur (see Démoulin, 2006, for a review). This has been shown to be the case in several observed flares (Démoulin *et al.*, 1997; Mandrini *et al.*, 1997; Bagalá *et al.*, 2000, and references therein). Following these previous studies, we propose that for the event analyzed quadrupolar reconnection occurred at QSLs, and more precisely at the location where they are the thinnest (called a hyperbolic flux tube by Titov, Hornig, and Démoulin, 2002), instead of being at a magnetic null point. Otherwise, the evolution predicted by the breakout model is consistent with our observations.

### 3.3. THE SMALL-SCALE QUADRUPOLAR EVENT

By exploring the coronal magnetic-field configuration, we find the presence of a 3D magnetic null point located at a height of 4.3 Mm above the photosphere over the negative polarity tongue (polarity 7). The vicinity of a null point can be described by the linear term in the local Taylor expansion of the magnetic field. The diagonalization of the Jacobian field matrix gives three orthogonal eigenvectors (Molodenskii and Syrovatskii, 1977). The divergence-free condition imposes that the sum of the three eigenvalues vanishes ($\lambda_1 + \lambda_2 + \lambda_3 = 0$). Furthermore, for

magnetic fields in equilibrium with a plasma ($\mathbf{j} \times \mathbf{B} = \nabla P$) the eigenvalues are real (Lau and Finn, 1990). Thus, two eigenvalues, say $\lambda_1$ and $\lambda_2$, have the same sign, which is opposite to that of the third eigenvalue ($\lambda_3$). The two spines of the null are defined by the two field lines that start at an infinitesimal distance from the null in directions parallel and anti-parallel to the eigenvector associated with $\lambda_3$. The fan surface is defined by all of the field lines starting at an infinitesimal distance from the null in the plane defined by the two eigenvectors associated with $\lambda_1$ and $\lambda_2$. For more information on magnetic nulls, see Greene (1988), Lau (1993), and Longcope (2006).

The magnetic null found in AR 10486 has two positive eigenvalues and one negative (null of type B; see, *e.g.*, Longcope, 2006). In this particular case, one of the fan eigenvalues is much larger than the other ($\sim$ five times larger). Then, starting from the null, most field lines in the fan plane bend in the directions parallel or anti-parallel to the eigenvector with the largest eigenvalue rather than tracing the full fan. To trace the full fan we would have to strongly increase the density of the field lines starting close to the directions parallel or anti-parallel to the eigenvector with the lowest eigenvalue, but we see no physical reason to do so. Rather, we start integrating field lines at small, but finite, distance from the null.

The characteristics of the null discussed above are a direct consequence of the nearby photospheric-field distribution. To illustrate this in the simplest possible way, we show in Figure 6 three theoretical configurations formed by four subphotospheric charges (at a depth of $z = -0.2$, below the plane representing the photosphere at $z = 0$). The intensities of the charges have been chosen to give a photospheric configuration similar to the observed one, *i.e.*, two strong, positive polarities and two, low-intensity, negative polarities (the positive charges are three times more intense than the negative ones). The positive ones are always located at $x = 0$, $y = \pm 1$, while the negative ones are always at $y = 0$ and are shifted in the $x$-direction from a symmetric location ($x = \pm 0.55$, model 1), to a more ($x = -0.3, 0.8$, model 2) and more ($x = -0.2, 0.9$, model 3) asymmetric one. The last model is closest to the observed configuration. As we go from model 1 to model 3, the largest fan eigenvalue is, respectively, two, three, and five times larger than the lowest eigenvalue. Because of this asymmetry, and to show some field lines along the lowest eigenvalue in the fan, we have drawn field lines starting at larger distances from the null in the third panel of Figure 6. Apart from that change, the null maintains the other characteristics, which are similar to the nulls in AR 10486, showing that it is structurally stable.

Figure 7 shows the magnetic null point in the observed configuration. If magnetic reconnection occurs at this magnetic null point, we expect to see two compact bright ribbons at the intersections of the spine with the photosphere and two additional ones, having an elongated shape, on the negative polarity between them (the photospheric trace of the fan). This is basically what TRACE observations at 1600 Å show (Figure 3, ribbons with a label starting with "r"); however, we have to be careful when associating different brightenings to different reconnection
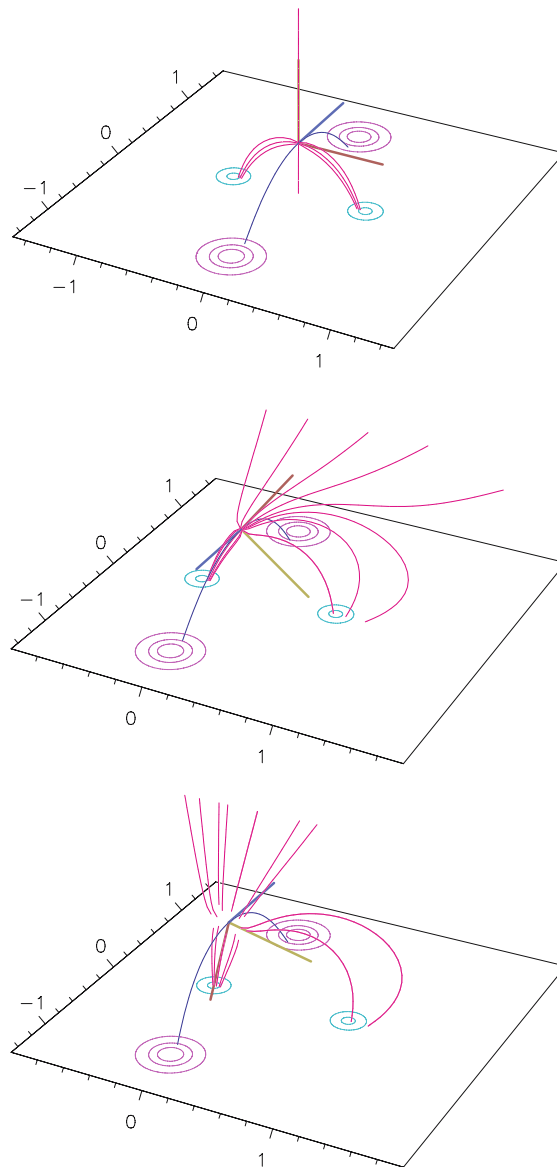
*Figure 6.* Coronal magnetic configuration in the vicinity of null points. The three panels correspond to the theoretical configurations (models 1, 2 and 3, respectively) discussed in Section 3.3. The three segments at the null locations correspond to the direction of the three eigenvectors of the Jacobian field matrix. The colors of the segments are indicative of the magnitude of each eigenvalue: *red* (*yellow*) corresponds to the largest (lowest) eigenvalue in the fan plane and *blue* to the spine eigenvalue. The yellow segment is vertical in the top figure and is overlapped with the red field line due to the symmetry of the configuration. The sign direction of the red and blue eigenvectors are reversed in the second panel, as compared to the other two, for better visualization. The red magnetic-field lines are drawn in the fan plane, while the blue line is the spine (all starting close to the null). In all figures the negative (positive) field isocontours are shown in *blue* (*pink*).
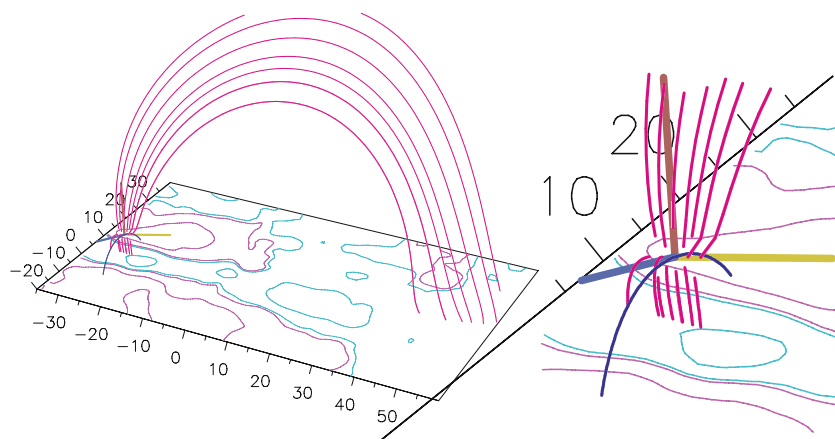
*Figure 7.* The *left panel* shows the magnetic null point in the observed AR 10486 coronal field. Field lines are starting in the close vicinity of the null point as in Figure 6. The *right panel* is an enlargement at the null location in which the direction of the three eigenvectors of the Jacobian field matrix are better seen. The axes are colored following the same convention as in Figure 6. The negative (positive) field isocontours are shown in *blue* (*pink*), their values are ±100, 1000 G.

processes since some loop structures also appear in this filter (for example, some reconnected loops, probably associated with the filament destabilization, lay at very low heights in the atmosphere).

The above conclusion is confirmed by computing field lines starting integration at the vicinity of the coronal null point, and taking into account its local topology. The left panel of Figure 8 corresponds to field lines before reconnection, while in the right panel they correspond to the ones after reconnection. Indeed, the shape
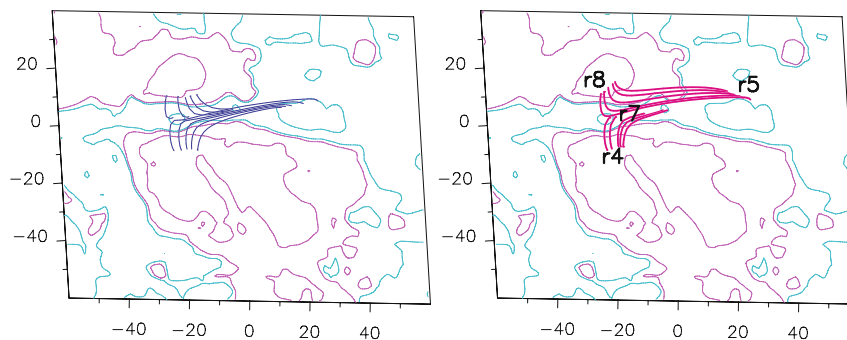


*Figure 8.* Coronal magnetic field model of AR 10486 in the vicinity of the magnetic null point. The *left panel* shows two sets of field lines representing the pre-reconnected lines (*blue*). The *right panel* corresponds to field lines after reconnection at the null point (*red*). The isocontours of the field are ±100, 1000 G, drawn with continuous *pink* (*blue*) lines for the positive (negative) values. The axes are labeled in Mm. The field of view is similar to the one shown in Figure 4. The approximate locations of the small-scale event ribbons are indicated in the *right panel* (see Figure 3).

of the last field lines follows closely the shape of the TRACE loops seen in 195 Å in Figure 4. Taking into account the magnetic field evolution (Section 2.2) and the computed coronal field topology, we propose that the magnetic null appears in the corona as polarities 7 and 8 emerged and grew in the pre-existing field of polarities 4 and 5 (Figure 1). Magnetic reconnection is driven by the local photospheric magnetic evolution.

Magnetic field reconnection at this null point is at the origin of the localized event discussed in Section 2.4, which started before and lasted as long as the X17 flare, being apparently independent from it. The very localized magnetic connectivities that we have described are a further indication that this small event was not a precursor of the X-flare. Reconnection at that null had only a local effect, without affecting the magnetic structure of the filament at the central part of the AR or the magnetic arcade above it.

A coronal null point was present at almost the same location on 27 October 2003 (Luoni, Mandrini, and Démoulin, 2006). Moreover, the bright loops observed by the Extreme Ultraviolet Telescope (SOHO/EIT) during the M6.7 flare on that day have the same shape as the loops seen by TRACE in 195 Å in our case. Régnier and Fleck (2004), using a non-linear, force-free field extrapolation of a magnetogram from the Imaging Vector Magnetograph, found a coronal magnetic null point at the same location on 27 October 2003. Since both the magnetic data (*i.e.*, time, instrument spatial resolution, and response function) and the extrapolation method are different, this gives further confidence that this magnetic null point is a stable topological structure where reconnection occurred independently from the X17 flare.

This result confirms that magnetic nulls are favorable regions for magnetic reconnection. They have been found associated with flares (*e.g.*, Gaizauskas *et al.*, 1999; Aulanier *et al.*, 2000; Fletcher *et al.*, 2001) but not in a systematic way (Démoulin, Hénoux, and Mandrini, 1994; Démoulin, 2006). Another piece of evidence for the presence of coronal nulls was given by Filippov (1999). He observed emission with the typical shape of a fan-spine structure near the limb and proposed that null points, where reconnection may occur, can be present in the corona (however, this shape can also be present without a null point as in Figure 5).

## 4. Discussion and Conclusions

Many studies have been devoted to AR 10486, since it produced many impressive eruptive events (Section 1). In such a complex AR, the events are also complex. Moreover, the presence of strong fields implies a large expansion of the eruptive configuration and, therefore, a strong interaction with neighboring fields (inside and even far outside the AR). AR magnetic fields are difficult to model when the magnetic stress in the region is very large. So such a complex AR, though highly interesting for solar–terrestrial relationships because of its CME production, is not well suited to understanding the elementary processes involved in an eruption.

However, with such strong events, and in particular such intense coronal magnetic fields, we could also expect to have strong precursors. Understanding what is happening long before the eruption is crucial to learning how the eruptive configuration is built up and how it is driven toward an instability. The pre-event phase has been analyzed in very few cases, partially because the precursor events are usually weak and buried within other secondary events (in particular, those participating in the coronal heating). Because of the strong fields in AR 10486, as well as the number of instruments devoted to its observation, we think that this example provides favorable conditions to analyze the precursors.

The presence of coronal magnetic nulls implies a complex topology, a configuration favorable for magnetic reconnection to occur. That is why their existence has been theoretically invoked as necessary for reconnection. We model the coronal field of AR 10486 using a linear, force-free approach, taking the observed longitudinal photospheric field as the boundary condition. Since the AR field is highly non-potential, the magnetic stress ($\alpha$ value) is set to the highest possible value for this type of computation. Using this model, we have found only one magnetic null above the chromosphere. It is located very low down in the corona, at a height of only four Mm above the photosphere. By computing field lines starting in its vicinity, we were able to reproduce the special shapes for two sets of observed coronal loops. Their particular shape is related to their location close to separatrices. We conclude that these small loops were formed by magnetic reconnection. The correspondence between the computed field lines, located in the vicinity of a magnetic null, with the observed loops validates *a posteriori* our magnetic extrapolation.

Have we found a precursor of the X17 flare due to reconnection at the magnetic null? We were initially very tempted to give a positive answer because this reconnection event started before the X-flare, at least about 1 hour earlier, and because it was located on the same magnetic inversion line, just to the east of the X-flare arcade. However, this small-scale event continued to be active during the X-flare without showing much change. Of course, the flare loops of the X-flare blurred the images, but we could find small loops with similar shapes before and during the X-flare. Thus, we conclude that reconnection at the magnetic null was not the trigger of the X-flare.

Apart from the just-described null point, we could not find another one. This could be due to the limitations of our extrapolation method, in particular, in this highly and non-uniformly magnetic-stressed case. However, the good correspondence between the computed field lines and coronal loops gives us the confidence that the extrapolation is able to find the right magnetic topology. Moreover, unless in specific cases (*e.g.*, Gorbachev *et al.*, 1988), coronal magnetic nulls are stable features (to modifications of the configuration). Finally, we have found no "bald patches" (Titov, Priest, and Démoulin, 1993) that could be linked to a precursor reconnection.

The above arguments would be suspicious if we had not found field lines linking the four main brightenings observed before the X-flare. Indeed, these field lines

are located in the vicinity where drastic changes in the magnetic connectivity are present, a configuration which is now common in flare analysis: a quadrupolar configuration where the classical separatrices are replaced by QSLs. Almost any evolution of such magnetic configuration will lead to the formation of strong current layers along the QSLs, as confirmed by recent MHD numerical simulations (Aulanier, Pariat, and Démoulin, 2005). As the magnetic stress increases, the current layers grow and become thinner until the dissipative scale length is reached. In these simulations, the strongest current sheets, and so the largest energy release, was attained with broader QSLs (because the storage phase could last longer before the dissipative lengths are reached). On top of the strong fields, the presence of QSLs, rather than separatrices, in AR 10486 could be at the origin of the important energy released in the quadrupolar reconnection before the X-flare. If separatrices would have been present, the dissipation scale length would have been reached much earlier, the magnetic energy would have been dissipated in much longer times, say days, with much less visible effects on the coronal plasma, so much less intense ribbons and loops would have occurred. The conclusion that quadrupolar reconnection could be best observed in configurations containing broad QSLs needs to be tested with further observations.

For the X17 flare on 28 October 2003, we have found a quadrupolar magnetic configuration where reconnection occurred and the stabilizing magnetic arcade above the filament configuration is progressively removed. This is similar to the breakout mechanism (Antiochos, DeVore, and Klimchuk, 1999), but without a magnetic null point. This study confirms previous ones: magnetic reconnection is not limited to cases with separatrices (a conclusion that probably also extends to the X17 flare). By studying only coronal null points, we would have only found the magnetic topology associated with the companion event.

# References

Alissandrakis, C.E.: 1981, *Astron. Astrophys.* **100**, 197.

Antiochos, S.K., DeVore, C.R., and Klimchuk, J.A.: 1999, *Astrophys. J.* **510**, 485.

Aulanier, G., Pariat, E., and Démoulin, P.: 2005, *Astron. Astrophys.* **444**, 961.

Aulanier, G., DeLuca, E.E., Antiochos, S.K., McMullen, R.A., and Golub, L.: 2000, *Astrophys. J.* **540**, 1126.

Bagalá, L.G., Mandrini, C.H., Rovira, M.G., and Démoulin, P.: 2000, *Astron. Astrophys.* **363**, 779.

Démoulin P.: 2006, *Adv. Space Res.* **37**, 1269.

Démoulin, P., Hénoux, J.C., and Mandrini, C.H.: 1994, *Astron. Astrophys.* **285**, 1023.

Démoulin, P., Hénoux, J.C., Priest, E.R., and Mandrini, C.H.: 1996, *Astron. Astrophys.* **308**, 643.

Démoulin, P., Bagalá, L.G., Mandrini, C.H., Hénoux, J.C., and Rovira, M.G.: 1997, *Astron. Astrophys.* **325**, 305.

Fan, Y. and Gibson, S.E.: 2004, *Astrophys. J.* **609**, 1123.

Filippov, B.: 1999, *Solar Phys.* **185**, 297.

Fletcher, L., Metcalf, T.R., Alexander, D., Brown, D.S., and Ryder, L.A.: 2001, *Astrophys. J.* **554**, 451.

Forbes, T.G. and Isenberg, P.A.: 1991, *Astrophys. J.* **373**, 294.

Gaizauskas, V., Mandrini, C.H., Démoulin, P., Luoni, M.L., and Rovira, M.G.: 1998, *Astron. Astrophys.* **332**, 353.

Gary, G.A. and Moore, R.L.: 2004, *Astrophys. J.* **611**, 545.

Gibson, S.E., Fan, Y., Mandrini, C.H., Fisher, G., and Démoulin, P.: 2004, *Astrophys. J.* **617**, 600.

Gorbachev, V.S., Kel'ner, S.R., Somov, B.V., and Shvarts, A.S.: 1988, *Sov. Astron.* **32**(3), 308.

Green, L.M., López Fuentes, M., Mandrini, C.H., Démoulin, P., van Driel-Gesztelyi, L., and Culhane, J.L.: 2002, *Solar Phys.* **208**, 43.

Greene, J.M.: 1988, *J. Geophys. Res.* **93**, 8583.

Hale, G.E. and Nicholson, S.B.: 1925, *Astrophys. J.* **62**, 270.

Handy, B.N., Acton, L.W., Kankelborg, C.C., *et al.*: 1999, *Solar Phys.* **187**, 229.

Harra, L.K., Démoulin, P., Mandrini, C.H., Matthews, S.A., van Driel-Gesztelyi, L., Culhane, J.L., and Fletcher, L.: 2005, *Astron. Astrophys.* **438**, 1099.

Kliem, B., Titov, V.S., and Török, T.: 2004, *Astron. Astrophys.* **413**, L23.

Klimchuk, J.A.: 2001, in P. Song, H. Singer, and G. Siscoe (eds.), *Space Weather* (Geophysical Monograph 125), Am. Geophys. Union, Washington, DC, p. 143.

Lau, Y.T.: 1993, *Solar Phys.* **148**, 301.

Lau, Y.T. and Finn, J.M.: 1990, *Astrophys. J.* **350**, 672.

Li, H., Schmieder, B., Aulanier, G., and Berlicki, A.: 2006, *Solar Phys.* (in press).

Lin, J., Forbes, T.G., Isenberg, P.A., and Démoulin, P.: 1998, *Astrophys. J.* **504**, 1006.

Longcope, D.W.: 2006, *Living Rev. Solar Phys.* **2**, *http://www.livingreviews.org/lrsp-2005-7*.

Luoni, M.L., Mandrini, C.H., and Démoulin, P.: 2006, *Bol. Asoc. Arg. Astron.* **48**, in press.

Mandrini, C.H., Démoulin, P., Bagalá, L.G., van Driel-Gesztelyi, L., Hénoux, J.C., Schmieder, B., and Rovira, M.G.: 1997, *Solar Phys.* **174**, 299.

Mein, P.: 2002, *Astron. Astrophys.* **381**, 271.

Metcalf, T.R., Jiao, L., McClymont, A.N., Canfield, R.C., and Uitenbroek, H.: 1995, *Astrophys. J.* **439**, 474.

Molodenskii, M.M. and Syrovatskii, S.I.: 1977, *Sov. Astron.* **21**, 734.

Pick, M., Malherbe, J.M., Kerdraon, A., and Maia, D.J.F.: 2005, *Astrophys. J.* **631**, L97.

Qiu, J. and Gary, D.E.: 2003, *Astrophys. J.* **599**, 615.

Régnier, S. and Fleck, B.: 2004, in R.W. Walsh, J. Ireland, D. Danesy, and B. Fleck (eds.), *ESA SP-575*, Proceedings of the SOHO 15 Workshop on Coronal Heating, ESA Publications Division, Noordwijk, The Netherlands, p. 519.

Scherrer, P.H., Bogart, R.S., Bush, R.I., Hoeksema, J.T., and Kosovichev, A.G., *et al.*: 1995, *Solar Phys.* **162**, 129.

Schmieder, B. and van Driel-Gesztelyi, L.: 2005, in K. Dere, J. Wang, and Y. Yan (eds.), *Coronal and Stellar Mass Ejections*, Proceedings of the IAU Symposium 226, Cambridge University Press, Cambridge, UK, p. 149.

Schmieder, B., Mandrini, C.H., Démoulin, P., Pariat, E., Berlicki, A., and DeLuca, E.E.: 2006, *Adv. Space Res.* **37**, 1313.

Titov, V.S., Hornig, G., and Démoulin, P.: 2002, *J. Geophys. Res.* **107**, SSH 3, 1.

Titov, V.S., Priest, E.R., and Démoulin, P.: 1993, *Astron. Astrophys.* **276**, 564.

Török, T. and Kliem, B.: 2005, *Astrophys. J.* **630**, L97.

van Driel-Gesztelyi, L., Schmieder, B., and Poedts, S.: 2002, in H. Sawaya-Lacoste (ed.), *ESA SP-477*, Proceedings of the Second Solar Cycle and Space Weather Euroconference, Solspa 2001, ESA Publications Division, Noordwijk, The Netherlands, p. 47.

Wang, H., Liu, C., Qiu, J., Deng, N., Goode, P.R., and Denker, C.: 2004, *Astrophys. J.* **601**, L195.

Williams, D.R., Török, T., Démoulin, P., van Driel-Gesztelyi, L., and Kliem, B.: 2005, *Astrophys. J.* **628**, L163.

Yurchyshyn, V., Hu, Q., and Abramenko, V.: 2005, *Space Weather* **3**, 8.

Zhang, H.-Q., Bao, X.-M., Zhang, Y., *et al.*: 2003, *Chin. J. Astron. Astrophys.* **3**, 491.